Journal of Alloys and Compounds 628 (2015) 195–198

Contents lists available at ScienceDirect

Journal of Alloys and Compounds

journal homepage: www.elsevier.com/locate/jalcom

Investigation of the microstructure and the influence of iron on the formation of Al_8Mn_5 particles in twin roll cast AZ31 magnesium alloy

S. Pawar [a,*], X. Zhou [a], T. Hashimoto [a], G.E. Thompson [a], G. Scamans [b,c], Z. Fan [b]

[a] School of Materials, The University of Manchester, Manchester M13 9PL, UK
[b] Brunel Centre for Advanced Solidification Technology (BCAST), Brunel University, Uxbridge, Middlesex UB8 3PH, UK
[c] Innoval Technology Ltd., Beaumont Close, Banbury, Oxon OX16 1TQ, UK

ARTICLE INFO

Article history:
Received 2 September 2014
Received in revised form 3 December 2014
Accepted 8 December 2014
Available online 24 December 2014

Keywords:
AZ31
Magnesium alloys
Transmission electron microscopy (TEM)
Iron
Intermetallics

ABSTRACT

The influence of iron on the formation of Al_8Mn_5 particles during twin roll casting of AZ31 magnesium alloy and the alloy microstructure has been investigated. Flower-shaped Al_8Mn_5 particles with sizes of 50–500 nm were observed at the grain centres and the grain boundaries. Additionally, Fe-particles with faceted morphologies and dimensions of less than 100 nm were observed at the centres of the Al_8Mn_5 particles, suggesting that the α-Fe particles acted as effective nucleation sites for the Al_8Mn_5 particles.

1. Introduction

Magnesium alloys have gained industrial attention from the automotive sector as attractive light weight structural materials, especially die-cast AZ series and AM series magnesium alloys [1,2]. However, cost-effectiveness in alloy processing has become increasingly important. The twin roll casting (TRC) process as a strip casting alternative exhibits several advantages including casting and rolling in a single step that result in improved microstructures with reduced grain sizes [3–5]. AZ31 Mg alloy, generally comprising 3 wt.% Al, 1 wt.% Zn and 0.2–0.5 wt.% Mn, has been widely exploited for commercial applications. It is well known that the alloying additions to magnesium lead to formation of intermetallics during solidification, where the cooling rates control the size, morphology and distribution of the intermetallics in the microstructure.

Manganese has been used as an alloying addition in Mg–Al based magnesium alloys, leading to the formation of Mn-containing intermetallic particles during solidification, which have been widely studied for their grain refining effect [6–8]. A further role of the manganese alloying addition in Mg–Al based magnesium alloys is to reduce the detrimental effect of iron on the alloy corrosion susceptibility [9]. Iron is inevitably present in magnesium alloy melts, which has been reported to precipitate in the form of iron particles or intermetallic compounds, Al–Fe or Al–Mn–Fe, during the solidification process [10,11]. Tamura et al. [12] observed cross-shaped Al–Mn–Fe particles after rapidly cooling the AZ91 magnesium alloy molten melt from superheating temperatures (900 °C). Cao and co-workers [10,13] reported the formation of Al-rich, Fe-rich and Mn-rich particles at the centres of the grains in Mg–Al based magnesium alloys. A duplex nucleation mechanism has also been reported that includes inoculation by Al_4C_3 particles which act as active nucleation sites for the formation of Al_8Mn_5 particles in the first stage; the Al_8Mn_5 particles further act as effective nucleation sites for the α-Mg grains in Mg–Al–Zn and Mg–Al–Mn magnesium alloys [14,15]. Kim et al. reported on the observation of Al–Mn dispersoid particles in the interdendritic regions, with irregular shapes and sizes ranging from 100 to 200 nm, in as-strip-cast ZMA6111 magnesium alloy [16].

Importantly, the formation mechanism of Al–Mn–Fe particles and their contribution to the grain refinement process are still the subject of discussion [17,18]. The present paper mainly focuses on the alloy microstructure and the influence of iron on the formation of Al_8Mn_5 intermetallic particles in the TRC AZ31 magnesium alloy. Advanced microscopy approaches have been employed in order to gain insight into the relationship between the presence of iron and the formation of Al_8Mn_5 intermetallic particles and their influence on the alloy microstructure, i.e. grain size.

* Corresponding author. Tel.: +44 1613065971.
E-mail address: surajkumar.pawar@manchester.ac.uk (S. Pawar).

http://dx.doi.org/10.1016/j.jallcom.2014.12.028
0925-8388/

2. Material and methods

AZ31 magnesium alloy strip sheets were produced by the conventional TRC process [4] and investigated in the as-cast condition. The alloy compositional analyses were performed using a Perkin–Elmer Optima 5300 dual view ICP-AES, confirming an iron content of 70 ppm in the alloy. Metallographic preparation was conducted by sequential mechanical polishing using 240–4000 grit SiC emery papers followed by polishing with 6, 3, 1 and ¼ μm diamond pastes with a non-aqueous lubricant. After polishing, the specimens were subjected to ultrasonic cleaning for 15–20 min. Scanning electron microscopy (SEM) of the alloy was performed using a PHILIPS XL30 field emission gun instrument, equipped with an energy dispersive spectroscopy (EDS) facility, at an accelerating voltage of 20 kV. Thin foils required for transmission electron microscopy (TEM) were mechanically ground and punched into 3 mm discs with an average thickness of less than 100 μm. The discs were ion beam thinned using a Gatan precision ion polishing system (PIPS) at 5.0 kV and at an incident angle of 4–6°. High resolution TEM was conducted on a Tecnai FEG F30 instrument operated at an accelerating voltage of 300 kV.

3. Results and discussion

The scanning electron micrograph of Fig. 1a displays the rolled surface of the TRC alloy, which comprises coarse dendritic grains of average grain size of ~600 μm. The general alloy microstructure reveals directional growth of dendritic grains, with an average value of the secondary dendrite arm spacing (SDAS) of ~7 μm. Evidence of rejected solute at the interface of the solidification fronts of the two adjacent dendritic grains is also revealed in the micrograph (indicated by arrows). Fig. 1b shows the components of the typical alloy microstructure, namely the α-Mg matrix, the $Mg_{17}Al_{12}$ phase, also termed the β-phase and Mn-rich intermetallic particles (both compositions determined by EDX as shown later). Ultra-fine lozenge-shaped β-precipitates, of <500 nm dimensions are clearly evident, close to the interdendritic regions in the bright field transmission electron micrograph of Fig. 1c. Fig. 1d shows a bright field transmission electron micrograph of the Mn-rich intermetallic particle, revealing its flower (rosette)-shaped morphology. Such Mn-rich intermetallic particles were observed at the centres of the α-Mg grains and the grain boundary regions (Fig. 1d). The Mn-rich particles have a sub-micron particle size, measuring 50–500 nm. The flower-shaped Mn-rich particles are significantly different from the description of the blocky/angular Mn-containing particles that are reported in literature [19]. The flower-shaped particle morphologies and the ultra-fine dimensions can be attributed to the relatively high cooling rates associated with the TRC process. It has been suggested that normal cooling rates can facilitate larger particle growth compared with the higher cooling rates that result in particle size refinement in the magnesium melts [3].

The SEM image and associated EDX elemental maps shown in Fig. 2 display the distributions of Mg, Zn, Al, Mn and Fe elements in the TRC alloy microstructure, and the distributions of the β-phase and Mn-rich particles in the α-Mg matrix. High Zn contents at the interdendritic regions suggest segregation of Zn during the solidification process. The elemental maps and the corresponding EDX analyses confirm that the flower-shaped particles are Mn-rich intermetallic particles.

The high angle annular dark field (HAADF) scanning transmission electron micrographs and the corresponding bright field images in Fig. 3 reveal the rosette-shaped Mn-rich particles from the sheet interior (Fig. 3a and b) and the flower-shaped particles on the rolled surface (Fig. 3c and d). The surface microstructure shows flat, (2D) dendrite-like, sub-micron sized growth of the particles (Fig. 3c and d) while the sheet interior displays a rosette morphology with multiple arms growing in all (3D) directions that form a globular structure (Fig. 3a and b). The difference in the particle morphologies are a consequence of the solidification intervals available for the growth of the particles. The high cooling rates on the rolled surfaces lead to rapid solidification that restricts the particle growth and results in fine particle sizes. In contrast, the sheet interior which experiences relatively low cooling rates, shows fully developed rosette-particle morphologies. The EDX analyses (Tables 1 and 2) at the points indicated in Fig. 3a and c revealed similar Al and Mn distributions in the two particles that are close to the

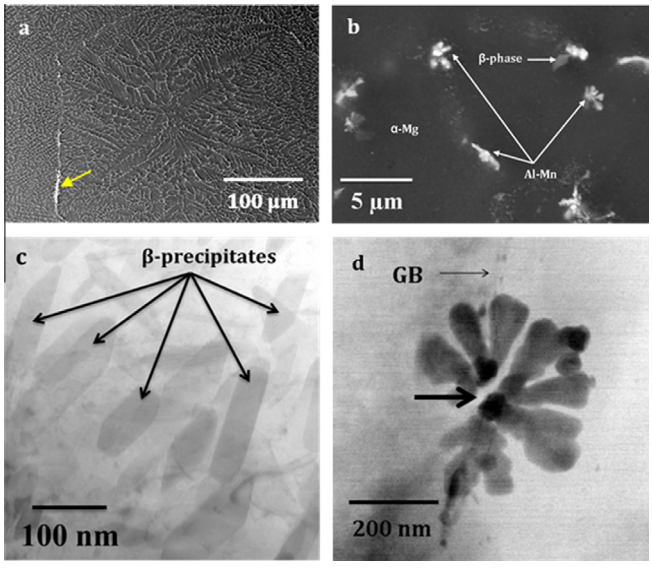

Fig. 1. (a) and (b) Backscattered scanning electron micrographs of the twin roll cast AZ31 magnesium alloy displaying the as-cast microstructure with a dendritic grain structure; (c) bright field TEM image revealing β-precipitates; and (d) bright field TEM image showing the Mn-rich particle at a grain boundary (GB).

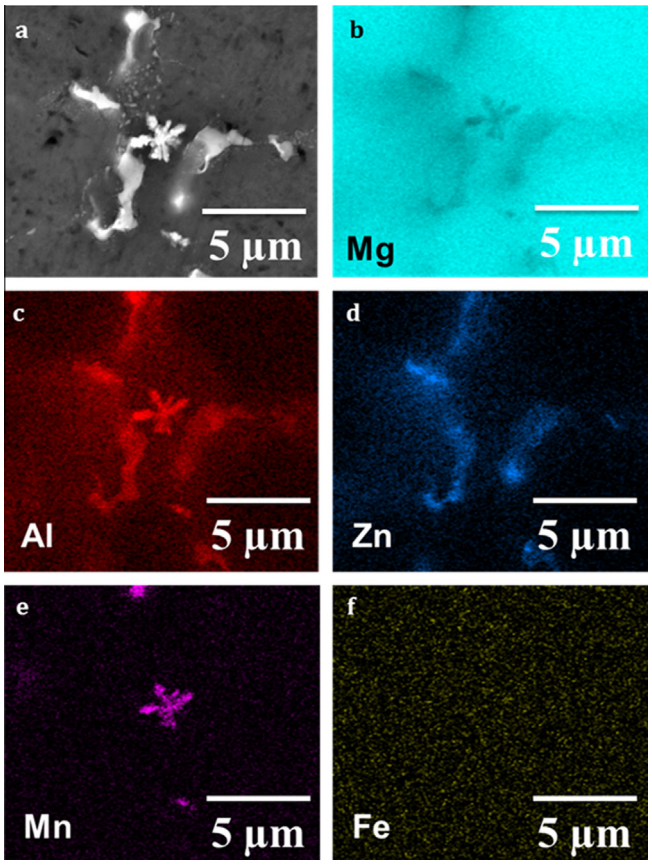

Fig. 2. (a) Secondary electron micrograph; and (b)–(f) EDX maps showing Mg, Al, Zn Mn and Fe elemental distributions respectively in the twin roll cast AZ31 Mg alloy.

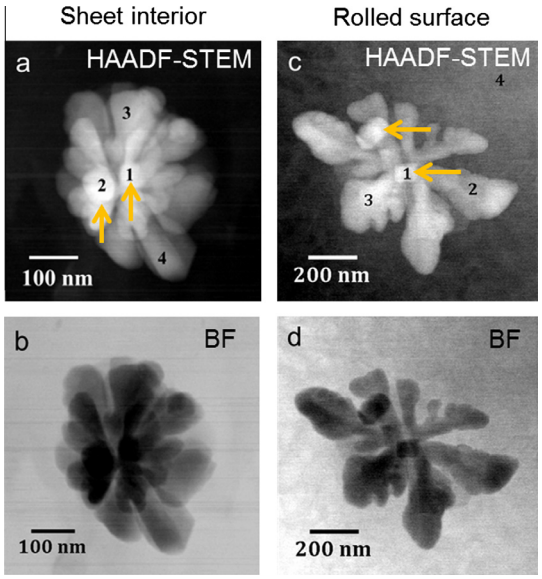

Fig. 3. (a) and (c) HAADF STEM images and (b) and (d) the corresponding bright field TEM images of the Al_8Mn_5 particles located in the twin roll cast AZ31 Mg alloy.

stoichiometric ratio of an Al_8Mn_5 intermetallic. Interestingly, it is evident from the transmission electron micrographs that there are individual nano-sized particles (appearing relatively dark in the bright field images and relatively bright in the HAADF images) (~50–150 nm), with faceted morphologies at the centres of the Al_8Mn_5 particles, as indicated by arrows. EDX analyses confirmed the presence of Fe at the faceted particles (points 1 and, 2 in Fig. 3a and point 1 in Fig. 3c). The Mg X-ray intensity arises from the surrounding magnesium matrix as a result of the relatively small size of the Al_8Mn_5 particle compared with the electron probe diameter. The significant difference between the X-ray interaction volume and the size of the faceted particles also suggest that the Fe contents in the particles could be significantly higher than that presented in the tables.

High resolution TEM analyses have been performed to ascertain the crystal structure of the flower-shaped intermetallic particles, nucleated on the faceted iron particle as shown in Fig. 4a with the lattice image revealed in Fig. 4b. The d-spacing values of 0.649 nm and 0.367 nm for the corresponding crystal planes of Al_8Mn_5 {0 1 2} and {1 2 2} respectively confirm the reported lattice parameters of a = 1.265 nm and c = 1.586 nm for the rhombohedral Al_8Mn_5 particle at ambient temperature [20]. Attempts were also made to determine the crystal structure of the faceted Fe particles at the centres of the Al_8Mn_5 particles. However, the relatively small size of the Fe particles compared to the specimen thickness prevented the acquisition of lattice images from the Fe particles.

Using PandaT simulation software and the thermodynamic data calculations from the latest PanMg8 database [21], self-cooling curves were generated under Schiel's condition which revealed the formation of Al_8Mn_5 intermetallic particles within a temperature regime of 635–631 °C. This is consistent with the previous report of the stable existence of Al_8Mn_5 particles in the temperature

Table 1
EDX point analyses acquired from the selected points indicated in Fig. 3a (at.%).

At.%	Mg	Al	Mn	Zn	Fe
Point 1	5.2	56.4	35.8	1.2	1.4
Point 2	8.1	53.9	35.3	1.1	1.6
Point 3	5.2	56.9	35.9	2.0	0.0
Point 4	6.4	56.1	36.8	0.7	0.0

Table 2
EDX point analyses acquired from the selected points indicated in Fig. 3c (at.%).

At.%	Mg	Al	Mn	Zn	Fe
Point 1	4.2	57.7	36.5	0.1	1.5
Point 2	4.0	58.1	37.5	0.4	0.0
Point 3	3.9	57.6	38.0	0.5	0.0
Point 4	96.3	2.8	0.0	0.9	0.0

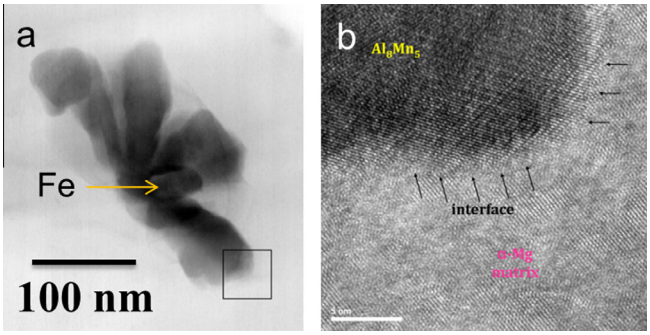

Fig. 4. (a) Bright field transmission electron micrograph of the flower shaped Al_8Mn_5 particle with a faceted Fe-particle and (b) high resolution TEM lattice image from the interface, highlighted in the framed region in (a).

range of 680–620 °C in a magnesium alloy containing 0.1–0.3 wt.% Mn [13]. The formation of Mn-containing particles in the early stages of the solidification process is due to the low solid solubility of manganese in magnesium melts [1]. The narrow temperature range over which Al_8Mn_5 formation occurs and the relatively high cooling rates associated with the TRC process, ranging from 10^2 to 10^3 K/s [3], both favour fine particle sizes since the solidification interval available for Al_8Mn_5 formation restricts growth of the particle. This is confirmed by the sub-micron particle sizes evident in Figs. 1 and 3.

Formation of stable bcc α-Fe particles in the magnesium melt at 649 °C was reported by Liu et al. [22]. In the present work, since the magnesium melt was held at 670 °C for 1 h, the formation of nano-sized primary Fe particles is considered to occur in the initial stages of the solidification process. The presence of these nano-sized Fe particles with "faceted edges" at the centres of the Al_8Mn_5 particles (as revealed in Figs. 1 and 3) clearly suggests that the Fe particles acted as nucleation sites for the formation of the Al_8Mn_5 intermetallics.

Further, from the current study, it is clear that the flower-shaped morphologies of the fine sized Al_8Mn_5 particles have the potential to act as effective nucleants for the α-Mg grains. However, precise investigation needs to be conducted in order to confirm the potency/efficacy of these Mn-containing particles. It is worth further investigation because these particles have ultra-fine sizes (50–500 nm) and their number density is relatively high (250 particles/cm^2), which is necessary for any potent nucleants to act as effective nucleating sites for the α-Mg grains.

4. Conclusions

1. Observation of "faceted" α-Fe particles with sizes less than 100 nm enclosed within the Al_8Mn_5 particles suggest that the Fe-particles act as active sites for the formation of the Al_8Mn_5 particles.
2. These Al_8Mn_5 particles, with typical rosette, flower and dendritic morphologies, and sub-micron particle sizes, were located at the grain centres, grain boundaries and the interdendritic regions.

3. The rolled surface showed a flat dendrite-like particle morphology, owing to the high cooling rates; while the sheet interior revealed a compete globular particle growth as a consequence of the low cooling rates of solidification.

Acknowledgements

The authors are grateful to the Engineering and Physical Sciences Research Council UK for support of the TARF-LCV Grant and the LATEST2 Programme Grant.

References

[1] O. Holta, H. Westengen, J. Roen, in: The 3rd International Magnesium Conference, Manchester, UK, 1996, pp. 75–87.
[2] J.J. Kim, D.H. Kim, K.S. Shin, N.J. Kim, Scr. Mater. 41 (1999) 333.
[3] Y.S. Park, S.B. Lee, N.J. Kim, Mater. Trans. 44 (2003) 2617.
[4] S.S. Park, Y.M. Kim, D.H. Kang, N.J. Kim, Mater. Sci. Forum 475–479 (2005) 457.
[5] S.S. Park, D.H. Kang, G.T. Bae, N.J. Kim, Mater. Sci. Forum 488–489 (2005) 431.
[6] C.E. Nelson, Trans. AFS 56 (1948) 1–23.
[7] N. Tiner, AIME Tech. Pub., vol. 12(7), 1945, pp. 1–19.
[8] Y. Tamura, T. Haitani, E. Yano, T. Motegi, N. Kono, E. Sato, Mater. Mater. Trans. A 33A (2002) 2784–2788.
[9] J.D. Hanawalt, C.E. Nelson, G.E. Holdeman, US Patent 2,267,862, 1940.
[10] P. Cao, M. Qian, D.H. StJohn, Scr. Mater. 51 (2004) 125–129.
[11] J.Y. Byun, S. Kwon, H.P. Ha, J.K. Yoon, in: K.U. Kainer (Ed.), Magnesium Alloys and Their Applications, Wiley-VCH, New York, NY, 2003, pp. 713–718.
[12] Y. Tamura, J. Yagi, T. Haitani, T. Motegi, N. Kono, H. Tamehiro, H. Saito, Mater. Trans. 44 (4) (2003) 552–557.
[13] P. Cao, M. Qian, D.H. StJohn, Scr. Mater. 54 (2006) 1853–1858.
[14] Y.M. Kim, C.D. Yim, B.S. You, Scr. Mater. 57 (2007) 691–694.
[15] S. Nimityongskul, M. Jones, H. Choi, R. Lakes, S. Kou, X. Li, Mater. Sci. Eng., A 527 (2010) 2104–2111.
[16] S.S. Park, Y.S. Oh, D.H. Kang, N.J. Kim, Mater. Sci. Eng., A 449–451 (2007) 352–355.
[17] T. Laser, M. Nurnberg, A. Janz, Ch. Hartig, D. Letzig, R. Schmid-Fetzer, R. Bormann, Acta Mater. 54 (2006) 3033–3041.
[18] M.X. Zhang, P.M. Kelly, M. Qian, J.A. Taylor, Acta Mater. 53 (2005) 3261–3270.
[19] S. Lun Sin, D. Dubé, R. Tremblay, Mater. Charact. 58 (2007) 989–996.
[20] JCPDS 2002. International Centre for Diffraction Data (#32-0021).
[21] Pandat is a software package for calculating phase diagrams and thermodynamic properties of multi-component alloys, CompuTherm LLC, 437 S. Yellowstone Dr. Suite 217, Madison, WI 53719 USA. Tel.:+1 (608) 274 1414; fax:+1 (608) 274 6045, info@computherm.com.
[22] M. Liu, P.J. Uggowitzer, A.V. Nagasekhar, P. Schmutz, M. Easton, G. Song, A. Atrens, Corros. Sci. 51 (2009) 602–619.